



1 **Transverse jointing in foreland fold-and-thrust belts: a remote sensing**
2 **analysis in the eastern Pyrenees**

3

4 Stefano Tavani¹, Pablo Granado², Amerigo Corradetti³, Thomas Seers³, Josep Anton Muñoz²

5

6 1 - DISTAR, Università degli Studi di Napoli “Federico II”, Via Cupa Nuova Cintia 21,
7 80126, Naples, Italy

8 2 - Institut de Recerca Geomodels, Departament de Dinàmica de la Terra i de l’Oceà,
9 Universitat de Barcelona, C/ Martí i Franques s/n, 08028, Barcelona, Spain

10 3 - Department of Petroleum Engineering, Texas A&M University at Qatar. Education City,
11 PO Box 23874, Doha, Qatar

12
13 **Abstract**

14 Joint systems in the eastern portion of the Ebro Basin of the eastern Pyrenees enjoy near
15 continuous exposure from the frontal portion of the belt up to the external portion of its
16 associated foredeep. Utilizing orthophoto mosaics of these world class exposures, we have
17 manually digitized over 30000 joints within a 16x50 km study area. The mapped traces
18 exhibit orientations that are dominantly perpendicular to the trend of the belt (transverse) and,
19 subordinately, orthogonal to it (longitudinal). In particular, joints systematically orient
20 perpendicular to the trend of the belt both in the frontal folds and in the inner and central
21 portion of the foredeep basin. Longitudinal joints occur rarely, with a disordered spatial
22 distribution, exhibiting null difference in abundance between the belt and the foredeep. Joint
23 orientations in the external portion of the foredeep become less clustered, with adjacent areas
24 dominated by either transverse or oblique joints. Our data indicates that joints in the studied
25 area formed in the foredeep in response to a foredeep-parallel stretching, which becomes
26 progressively less intense within the external portion of the foredeep. There, the minimum
27 stress direction becomes more variable, evidencing poor contribution of the forebulge-
28 perpendicular stretching on stress organization.

29



1 Introduction

2 Fractures can be effective pathways for fluid flow (e.g. Laubach et al., 2019), thus
3 impacting production of hydrocarbons (Barr et al., 2007; Engelder et al., 2009; Questiaux et
4 al., 2010) and geothermal water (Haffen et al., 2013; Vidal et al., 2017), the pathways and
5 fates of contaminants released from deep geological radioactive waste repositories
6 (Berkowitz et al., 1988; Iding and Ringrose, 2010) and the sustainable management of
7 groundwater (Masciopinto and Palmiotta, 2013). Associated with crustal tension, joints are
8 ubiquitous open-mode fractures occurring in a range of tectonic settings, including collisional
9 belts. In collisional settings, layer bending and stretching during the growth of thrust-related
10 anticlines has conventionally been invoked as the principal causative process for the
11 development of joints oriented approximately parallel (e.g. Ramsay, 1967; Murray, 1968) and
12 perpendicular (e.g. Dietrich, 1989; Lemiszki et al., 1994) to the trend of the belt and of the
13 thrust related anticlines. However, the frequently observed obliquity between joints (and
14 other meso-scale structures) and the trend of the hosting anticlines (e.g. Tavani et al., 2019;
15 Beaudoin et al., 2020), along with the documented occurrence of joints in exposed forelands
16 (e.g. Dunne and North, 1990; Zhao and Jacobi, 1997; Billi and Salvini, 2003; Whitaker and
17 Engelder, 2006), has more recently led to the conclusion that, in many cases, joints and other
18 kinds of extensional fractures exposed in thrust and fold belts have developed prior to folding
19 and thrusting, within the foreland region (e.g. Doglioni, 1995; Zhao and Jacobi, 1997;
20 Tavarnelli and Peacock, 1999; Lash and Engelder, 2007; Branellec et al., 2015; Basa et al.,
21 2019; Giuffrida et al., 2019; Martinelli et al., 2019; Carrillo et al., 2020), where joints are
22 layer-perpendicular and commonly oriented parallel (longitudinal) and perpendicular
23 (transverse) to the belt-foredeep-forebulge trend (Tavani et al., 2015).

24 A partially unresolved question in foreland deformation relates to the development of
25 transverse joints, which requires a tensile minimum stress oriented parallel to the foredeep.
26 Even in arched systems, the forebulge, the foredeep, and the belt tend to be nearly parallel to
27 each other locally. The shortening direction in the inner portion of the foredeep (subjected to
28 layer parallel shortening) and the stretching direction in the forebulge (where bulge-
29 perpendicular stretching induced by lithospheric outer arc extension operates) are nearly
30 parallel in a belt-perpendicular transect (Fig. 1). In addition, in the innermost portion of the
31 foredeep, where layer parallel shortening operates, the σ_2 is typically vertical and the σ_3 is
32 positive, horizontal, and parallel to the trend of the belt (Tavani et al., 2015). Given the



1 above, there should be an area in between the inner portion of the foredeep and the peripheral
2 bulge where σ_1 becomes vertical and where σ_3 is still horizontal and parallel to the belt (Fig.
3 1a). This scenario could explain the development of layer-perpendicular transverse
4 extensional structures, with transverse extensional faults or veins expected to develop where
5 σ_3 is positive. In this scenario, transverse joints occurring in this zone of localized tension
6 could only develop as cross-joints (e.g. Gross, 1993) of the longitudinal set formed in the
7 forebulge. This simplified model does not explain the documented occurrence of transverse
8 joints in areas where longitudinal joints do not occur or represent the cross-joint set (e.g.
9 Zhao and Jacobi, 1997; Quintà and Tavani, 2012). This framework does not admit a simple
10 stress permutation in the foredeep and requires a negative σ_3 connected to a foredeep-parallel
11 stretching component (Fig. 1b). Lithospheric bending of the foredeep, both along the
12 horizontal plane (e.g. Doglioni, 1995) and along the vertical plane parallel to the trench
13 (Quintà and Tavani, 2012), has been invoked as a process able to produce foredeep-parallel
14 stretching.

15 Continuous exposures across the entire foreland region of the eastern Pyrenees allows
16 investigation of the primary mechanism responsible for transverse joint development
17 described above. Tens to hundreds of meters long joints affect the sedimentary sequence of
18 the Ebro foredeep basin (Fig. 2a), and are found tilted within the frontal structures of the
19 Pyrenean belt (Fig. 2b). These pre-folding joints are exceptionally exposed and mappable
20 from orthophotos (Fig. 2c-f), from which they can be traced almost continuously from the
21 external portion of the foredeep until the thrust belt. We have remotely mapped 30059 joints
22 traces from the aforementioned orthophoto dataset and obtained their azimuthal distributions
23 across the study area. Subsequently, this extended lineament database has been used to
24 constrain causative mechanism behind transverse jointing in the Ebro foredeep basin.

25

26 **Geological Setting**

27 The study area is situated in the eastern Ebro foreland basin within an area connecting
28 the eastern Pyrenees with the Catalan Coastal Ranges (Fig. 3a). The Pyrenees is an EW-
29 striking orogenic system that formed as the Iberian and European plates collided from Late
30 Cretaceous to Miocene times (Roest and Srivastava, 1991; Rosenbaum et al., 2002; Muñoz,
31 1992, 2002), and constitute an asymmetric, doubly vergent orogenic wedge above the
32 northward subduction of the Iberian lithosphere beneath the European plate (Chevrot et al.,



1 2018). As a result, the Ebro basin formed as a flexural foreland developed on the downgoing
2 Iberian plate at the southern margin of the chain (Beaumont et al., 2000). In the study area, to
3 the south of the Ebro Basin (Fig. 3a), the Catalan Coastal Ranges developed as a Paleogene
4 intraplate left-lateral transpressional system (López-Blanco, 2002; Santanach et al., 2011).
5 The low-displacement character of thrusts and the absence of an associated foredeep both
6 evidence the limited importance of this range. A series of NE-SW and NW-SE trending
7 extensional faults strike parallel and perpendicular to the Catalan Coastal Range respectively,
8 which are a result of the late Oligocene-Miocene opening of the NW Mediterranean basin
9 (Vegas, 1992; Sàbat et al., 1995; Granado et al., 2016a).

10 The study area where joint traces have been digitized is delimited to the north by the
11 frontal Pyrenean thrusts and by the Eocene Bellmunt anticline (Figs. 3a,b). This anticline
12 comprises the Paleocene to upper Eocene foredeep infill. Immediately to the south of the
13 anticline (i.e. < 5 km), this multilayer becomes sub-horizontal and thins southward where the
14 Paleozoic to Mesozoic foredeep floor gently rises up southward and becomes exposed (Fig.
15 3a). There, this Paleozoic to Cenozoic succession is slightly tilted to the north by uplift in the
16 footwall of NW-SE striking Late Oligocene to Neogene extensional faults. Further to the
17 southwest, this succession is affected by the Paleogene contractional structures of the Catalan
18 Coastal Ranges (Fig. 3b).

19

20 **Data and Methods**

21

22 Joints have been digitized within the 16.4x49.2 km area displayed in Figure 3, on 25
23 and 50 cm/px orthophotos provided by the Spanish Instituto Geografico Nacional via the
24 PNOA (Plan Nacional de Ortofotografía Aérea) project (<https://pnoa.ign.es/>). The open
25 source geographical information system QGIS 3.4 has been used to manually digitize 30059
26 joint traces. A collection of these traces seen on orthophotos is provided in Figure 2c-f. Joints
27 have been digitized in Bartonian and, subordinately, in Lutetian and Priabonian sedimentary
28 rocks (Fig. 3c). The NE and SE portions of the study area are highly vegetated (Fig. 3d,e) and
29 only a few joint traces have been mapped there. Quaternary sediments unaffected by joints
30 crop out in the central portion of the study area (Fig. 3d).

31 Digitized traces have lengths ranging from 2 to 100 m, with an average of ~20 m (Fig.
32 3f). The frequency distribution of trace trend shows that the vast majority of the mapped



1 joints are approximately N-S striking (Fig. 3f). A second subordinate set corresponds to E-W
 2 striking joints, which in the field occur as cross-joints (Fig. 2d). The frequency distribution of
 3 trace trend is not symmetrical around these orthogonal sets, due to the presence of a third less
 4 abundant set composed of NW-SE oriented joints (Fig. 2e,f). The NW-SE striking joints are
 5 mostly seen in the southern portion of the study area, in exposures where the N-S striking set
 6 is not occurring. Generally speaking, exposures are mostly characterized by a single set (Fig.
 7 3c,d). At a few locations, the dominant set is accompanied by associated cross-joints (Fig.
 8 3d). Very rarely, two mutually oblique sets occur in the same exposure (Fig. 2f).

9 In order to evaluate the variability of joint traces, the 16.4x49.2 km study area has
 10 been divided into meshes of equilateral triangular elements with edge lengths of 1025m
 11 (Mesh 1) and 1640m (Mesh 2). At each node, mean value and variance of trace trends has
 12 been computed using a circular moving window with a radius of 1200m (Mesh 1) and 1900m
 13 (Mesh 2). Since trace trends are circular data with an angle (α) over a period π , in agreement
 14 with Mardia (1975) we used equations 1 to 4 to derive at each node the circular mean value
 15 (Mv_{π}), the circular variance (V_{π}) and the resultant length (R_{π} ; $V_{\pi} = 1 - R_{\pi}$), the latter spanning
 16 from 0 (unclustered distribution) to 1 (perfectly clustered distribution). In the presence of
 17 cross-orthogonal joint sets, it is also useful using a period of $\pi/2$, thus modifying Mardia's
 18 equations and introducing the $Mv_{\pi/2}$ and $R_{\pi/2}$ parameters, which are computed using Equations
 19 5 to 8.

20

$$C_{\pi} = \frac{\sum_{i=1}^n \cos(2\alpha_i)}{n} \quad (1); \quad S_{\pi} = \frac{\sum_{i=1}^n \sin(2\alpha_i)}{n} \quad (2); \quad V_{\pi} = 1 - R_{\pi} = 1 - \sqrt{C_{\pi}^2 + S_{\pi}^2} \quad (3); \quad Mv_{\pi} = \frac{\text{Arctan}(S_{\pi}/C_{\pi})}{2} \quad (4)$$

$$C_{\pi/2} = \frac{\sum_{i=1}^n \cos(4\alpha_i)}{n} \quad (5); \quad S_{\pi/2} = \frac{\sum_{i=1}^n \sin(4\alpha_i)}{n} \quad (6); \quad V_{\pi/2} = 1 - R_{\pi/2} = 1 - \sqrt{C_{\pi/2}^2 + S_{\pi/2}^2} \quad (7); \quad Mv_{\pi/2} = \frac{\text{Arctan}(S_{\pi/2}/C_{\pi/2})}{4} \quad (8)$$

21
 22

23 By using these four parameters together, instead for example of the classical k-means
 24 clustering analysis, it is possible to derive important considerations on the distribution of
 25 polymodal distributions in which two mutually orthogonal sets do occur, as illustrated in
 26 Figure 4. We compare the Mv and the R parameters computed using the π and $\pi/2$ periods. In
 27 the first example two parallel traces are analyzed, resulting in $Mv_{\pi/2} = Mv_{\pi}$, and $R_{\pi/2} = R_{\pi} = 1$
 28 (i.e. circular variance = 0). When data dispersion is slightly increased (Example 2), $Mv_{\pi/2}$ is
 29 still equal to Mv_{π} , whereas $R_{\pi/2}$ decreases faster than R_{π} . Further increase of data dispersion
 30 (Example 3), in an asymmetric distribution (i.e. non-orthogonal sets), causes additional



1 decrease of $R_{\pi/2}$ with respect to R_{π} , and slight divergence between $Mv_{\pi/2}$ and Mv_{π} . In the
2 presence of a cross-orthogonal subset, the statistical usefulness of $R_{\pi/2}$ becomes evident, as
3 illustrated in Example 4. In this case, R_{π} rapidly approaches zero, suggesting high dispersion
4 (i.e. unrepresentative Mv_{π}), whereas $R_{\pi/2}$ is essentially unaffected with respect to Example 2,
5 indicating low dispersion and a representative $Mv_{\pi/2}$. However, the use of the $\pi/2$ period only
6 returns results in the 0 to $\pi/2$ range, so that NW-SE trending traces result in a NE-SW
7 trending mean value ($Mv_{\pi/2}$), as shown in the Example 5. In summary, Mv_{π} is useful to derive
8 the mean direction, whereas $R_{\pi/2}$ and R_{π} should be used in conjunction to discriminate
9 between populations in which oblique sets occur ($R_{\pi/2} < R_{\pi}$) from those in which two
10 perpendicular sets occur ($R_{\pi/2} > R_{\pi}$).

11

12 Results

13 Figure 5 displays attribute maps generated from Mesh 1 and Mesh 2 using the trace
14 orientation parameters described above. Both Mesh 1 and Mesh 2 have $R_{\pi} > 0.5$ across almost
15 the entirety of the study area, with the only exception being in the NW corner of the study
16 area. For $R_{\pi/2}$, in addition to the NW corner, the central portion of the study area has $R_{\pi/2} <$
17 0.5. Noteworthy differences between R_{π} and $R_{\pi/2}$ occur: (1) in the NW corner ($R_{\pi} \ll R_{\pi/2}$) and
18 (2) in the central area ($R_{\pi} \gg R_{\pi/2}$). The first area corresponds to a vegetated folded and faulted
19 area (Fig 3b-e). Consequently, we consider the dataset poorly reliable in this location. In the
20 central portion of the study area, the difference between R_{π} and $R_{\pi/2}$ (which increases as data
21 dispersion increases) is less pronounced in Mesh 1 than Mesh 2. Thus, data dispersion
22 increases with increasing the search window size (1200m for Mesh 1 and 1900m for Mesh 2),
23 evidencing that joint orientation is changing in this area. In the rest of the analyzed foreland,
24 $R_{\pi/2}$ has values similar to R_{π} , indicating approximately unimodal data distribution within this
25 region, and poor spatial organization of the longitudinal cross-joints.

26 Distribution of Mv_{π} relates to the prevalence of NS-striking joints in the northern and
27 central portion of the study area. Towards the south, patches characterized by both N-S and
28 NW-SE-striking joints occur. High values of R_{π} and $R_{\pi/2}$ are characteristic of such subareas,
29 which as previously mentioned, is indicative of unimodal joint trace distributions.

30

31 Discussion



1 Remotely sensed and mapped joint traces in the eastern portion of the Pyrenees-Ebro
2 system show systematic distributions of azimuthal orientations. In the frontal portion of the
3 belt and within the foredeep, joints are mostly transverse (i.e. N-S-striking), with limited
4 occurrence of E-W-striking longitudinal cross-joints. Approaching the southern border of the
5 foredeep, joints exhibit both N-S and NW-SE orientations where the pre-Cenozoic floor of
6 the foredeep is exposed. Joints affect Lutetian to Priabonian foredeep infill, and are found
7 tilted together with strata within the Bellmont anticline (Fig. 2b), which is Priabonian in age
8 (Burbank et al., 1992). Given the above, the timing of jointing in the area must be during or
9 before the Priabonian. Evidencing this proposed framework, there are no systematic and
10 pervasive joints affecting Quaternary sediments (Fig. 3), while Oligo-Mio-Pliocene
11 sediments are not present in the rock record of the studied area. The occurrence of the N-S
12 striking joints within the Ebro foredeep is documented also to the west of the study area (e.g.
13 Turner and Hancock, 1990), where joint emplacement affects up to the Miocene (Arlegui and
14 Simon, 2001). Transverse joints, striking approximately NNE-SSW occur also to the SW in
15 the Bartonian to Priabonian strata cropping out at the boundary between the Ebro basin and
16 the Catalan Coastal Ranges (Alsaker et al., 1996). These data indicate that transverse joints
17 systematically developed in the foredeep basin of the E-W oriented Pyrenean belt. Locally,
18 the process of transverse jointing occurred until the Miocene (i.e. until the end of mountain
19 building). Also, pre-thrusting transverse extensional faults of upper Paleocene to lower
20 Eocene age occur a few tens of km to the NE of the study area (Carrillo et al., 2020), being
21 presently incorporated into the Pyrenean belt. Thus, we conclude that foredeep-parallel
22 extension has occurred in the foredeep of the Pyrenean belt since the Paleocene and until the
23 end of convergence. Transverse joints documented in this work clearly represent foredeep-
24 related structures (Tavani et al., 2015). The relatively constant orientation of joints along the
25 strike of the foredeep, the occurrence of appreciable dispersion at the outer border of the
26 foredeep, and the remarkably poor abundance of longitudinal joints allow us to derive two
27 major conclusions:

28 (1) The almost linear trend of the Pyrenees facilitates the exclusion of planar arching (e.g.
29 Doglioni, 1995; Zhao and Jacobi, 1997) as the causative process for generating foredeep-
30 parallel stretching (i.e. required to establish the negative σ_3 responsible for transverse
31 jointing). Arching along the vertical plane parallel to the trench (Quintà and Tavani, 2012)
32 represents instead a viable mechanism for generating along-foredeep stretching. This is



1 analogous, albeit at a larger scale to the process of release faulting described by Destro
2 (1995), and requires a laterally decreasing depth of the foredeep, which is confirmed by the
3 westward plunge of the foredeep basin in the study area (Fig. 3a).

4 (2) Extension in the peripheral bulge, which is documented from many active and fossil
5 foredeep basins (e.g. Bradley and Kidd, 1991; Ranero et al., 2003; Tavani et al., 2015;
6 Granado et al., 2016b), including the lower Eocene foredeep basin presently incorporated into
7 the Pyrenees (e.g. Martinez et al., 1989; Pujadas et al., 1989) appears to be weakly influential
8 at the southern border of the study area (i.e. the upper Eocene peripheral bulge). Indeed, the
9 observed longitudinal joints are characteristically subordered, forming locally as cross-joints
10 to the identified transverse set within the study area (Fig. 2d). The transverse set becomes less
11 organized at the southern margin of the foredeep, where patches of N-S and NW-SE
12 dominated domains do occur. This evidences the absence of a major forebulge-perpendicular
13 extension capable of systematically reorienting σ_3 at the external foredeep edge.

14

15 **Conclusions**

16 Analysis of remotely sensed and mapped joints in the eastern Pyrenees and in the
17 adjacent Ebro foreland basin indicates that the emplacement of the dominant joint set within
18 the area, which strikes perpendicular to the trend of the foredeep occurred prior to folding
19 and developed in response to along-strike stretching caused by the plunging shape of the
20 foredeep. Joints developed in response to flexuring of the lithosphere at the peripheral bulge
21 do not occur in the area, suggesting that this mechanism has limited relevance to the observed
22 joint system. This is confirmed by the variability of joint orientations observed at the
23 foredeep external edge, negating the occurrence of a major forebulge-perpendicular extension
24 able to systematically orient the stress field at the foredeep edge.

25

26

27

28

29 **Data availability**

30 Digitized traces in shapefile format are in the supplementary materials

31

32 **Author contributions**



1 ST, PG, AC, TS, and JAM contributed equally to the elaboration of the manuscript.

2

3 **Competing interests**

4 The authors declare that they have no conflict of interest.

5

6 **Acknowledgements**

7 The Institut de Recerca Geomodels and the Geodinàmica i Anàlisi de Conques research
8 group (2014SGR467SGR) acknowledges financial support from the Agència de Gestió
9 d'Ajuts Universitaris i de Recerca (AGAUR) and the Secretaria d'Universitats i Recerca del
10 Departament d'Economia i Coneixement de la Generalitat de Catalunya.

11

12 **References**

- 13 Alsaker, E., Gabrielsen, R. H., and Roca, E.: The significance of the fracture pattern of the
14 Late-Eocene Montserrat fan-delta, Catalan Coastal Ranges (NE Spain),
15 Tectonophysics, 266, 465-491, [https://doi.org/10.1016/S0040-1951\(96\)00239-9](https://doi.org/10.1016/S0040-1951(96)00239-9), 1996
- 16 Arlegui, L., and Simón, J. L.: Geometry and distribution of regional joint sets in a non-
17 homogeneous stress field: case study in the Ebro basin (Spain), Journal of Structural
18 Geology, 23, 297-313, [https://doi.org/10.1016/S0191-8141\(00\)00097-3](https://doi.org/10.1016/S0191-8141(00)00097-3), 2001
- 19 Barr, D., Savory, K.E., Fowler, S.R., Arman, K., and McGarrity, J.P.: Pre-development
20 fracture modelling in the Clair field, west of Shetland, Geol. Soc. Lond. Special
21 Publication, 270, 205-225, <https://doi.org/10.1144/GSL.SP.2007.270.01.14>, 2007
- 22 Basa, A., Ahmed, F., Bhattacharyya, K., and Roy, A.: Evolution and characterization of
23 fracture patterns: Insights from multi-scale analysis of the Buxa dolomite in the Siang
24 Valley, Arunachal Lesser Himalayan fold-thrust belt. Journal of Structural Geology,
25 123, 54-66, <https://doi.org/10.1016/j.jsg.2019.03.004>, 2019
- 26 Beaumont, C., Muñoz, J. A., Hamilton, J., and Fullsack, P.: Factors controlling the Alpine
27 evolution of the central Pyrenees inferred from a comparison of observations and
28 geodynamical models, Journal of Geophysical Research: Solid Earth, 105, 8121-
29 8145, <https://doi.org/10.1029/1999JB900390>, 2000
- 30 Beaudoin, N, Lacombe, O, David, M-E, and Koehn, D.: Does stress transmission in forelands
31 depend on structural style?. Distinctive stress magnitudes during Sevier thin-skinned



- 1 and Laramide thick-skinned layer-parallel shortening in the Bighorn Basin (USA)
2 revealed by stylolite and calcite twinning paleopiezometry, *Terra Nova*, [https://doi.org/](https://doi.org/10.1111/ter.12451)
3 [10.1111/ter.12451](https://doi.org/10.1111/ter.12451), 2020
- 4 Berkowitz, B., Bear, J., and Braester, C.: Continuum models for contaminant transport in
5 fractured porous formations, *Water Resour. Res.*, 24, 1225-1236,
6 <https://doi.org/10.1029/WR024i008p01225>, 1988
- 7 Billi, A., and Salvini, F.: Development of systematic joints in response to flexure-related fibre
8 stress in flexed foreland plates: the Apulian forebulge case history, Italy, *Journal of*
9 *Geodynamics*, 36, 523-536, [https://doi.org/10.1016/S0264-3707\(03\)00086-3](https://doi.org/10.1016/S0264-3707(03)00086-3), 2003
- 10 Bradley, D. C., and Kidd, W. S. F.: Flexural extension of the upper continental crust in
11 collisional foredeeps, *Geological Society of America Bulletin*, 103, 1416-1438, [https://](https://doi.org/10.1130/0016-7606(1991)103<1416:FEOTUC>2.3.CO;2)
12 [doi.org/10.1130/0016-7606\(1991\)103<1416:FEOTUC>2.3.CO;2](https://doi.org/10.1130/0016-7606(1991)103<1416:FEOTUC>2.3.CO;2), 1991
- 13 Branellec, M., Callot, J. P., Nivière, B., and Ringenbach J. C.: The fracture network, a proxy
14 for mesoscale deformation: Constraints on layer parallel shortening history from the
15 Malargüe fold and thrust belt, Argentina, *Tectonics*, 34, 623-647,
16 <https://doi.org/10.1002/2014TC003738>, 2015
- 17 Burbank, D. W., Puigdefàbregas, C., and Muñoz, J. A.: The chronology of the Eocene
18 tectonic and stratigraphic development of the eastern Pyrenean foreland basin,
19 northeast Spain, *Geological Society of America Bulletin*, 104, 1101-1120,
20 [http://doi.org/10.1130/0016-7606\(1992\)104<1101:TCOTET>2.3.CO;2](http://doi.org/10.1130/0016-7606(1992)104<1101:TCOTET>2.3.CO;2), 1992
- 21 Carrillo, E., Guinea, A., Casas, A., Rivero, L., Cox, N., and Vázquez-Taset, Y. M.: Tectono-
22 sedimentary evolution of transverse extensional faults in a foreland basin: Response to
23 changes in tectonic plate processes. *Basin Research*, <https://doi.org/10.1111/bre.12434>,
24 2020
- 25 Chevrot, S., Sylvander, M., Díaz, J., Martin, R., Mouthereau, F., Manatschal, G., Masini, E.,
26 Calassou, S., Grimaud, F., Pauchet, H., and Ruiz, M.: The non-cylindrical crustal
27 architecture of the Pyrenees, *Scientific Reports*, 8, 9591,
28 <https://doi.org/10.1038/s41598-018-27889-x>, 2018
- 29 Destro, N.: Release fault: A variety of cross fault in linked extensional fault systems, in the
30 Sergipe-Alagoas Basin, NE Brazil, *Journal of Structural Geology*, 17, 615-629, [https://](https://doi.org/10.1016/0191-8141(94)00088-H)
31 [doi.org/10.1016/0191-8141\(94\)00088-H](https://doi.org/10.1016/0191-8141(94)00088-H), 1995



- 1 Dietrich, D.: Fold-axis parallel extension in an arcuate fold-and thrust belt: the case of the
2 Helvetic nappes. *Tectonophysics*, 170, 183-212, [https://doi.org/10.1016/0040-](https://doi.org/10.1016/0040-1951(89)90271-0)
3 [1951\(89\)90271-0](https://doi.org/10.1016/0040-1951(89)90271-0), 1989
- 4 Doglioni, C.: Geological remarks on the relationships between extension and convergent
5 geodynamic settings, *Tectonophysics*, 252, 253-267. [https://doi.org/10.1016/0040-](https://doi.org/10.1016/0040-1951(95)00087-9)
6 [1951\(95\)00087-9](https://doi.org/10.1016/0040-1951(95)00087-9), 1995
- 7 Dunne, W. M., and North, C. P.: Orthogonal fracture systems at the limits of thrusting: an
8 example from southwestern Wales, *Journal of Structural Geology*, 12, 207-215, [https://](https://doi.org/10.1016/0191-8141(90)90005-J)
9 [doi.org/10.1016/0191-8141\(90\)90005-J](https://doi.org/10.1016/0191-8141(90)90005-J), 1990
- 10 Engelder, T., Lash, G.G., and Uzcategui, R.: Joint sets that enhance production from Middle-
11 Upper Devonian gas shales of the Appalachian basin, *AAPG Bull.*, 93, 857-889,
12 <https://doi.org/10.1306/03230908032>, 2009
- 13 Giuffrida, A., La Bruna, V., Castelluccio, P., Panza, E., Rustichelli, A., Tondi, E., Giorgioni,
14 M., Agosta, F.: Fracture simulation parameters of fractured reservoirs: Analogy with
15 outcropping carbonates of the Inner Apulian Platform, southern Italy, *Journal of*
16 *Structural Geology*, 123, 18-41, <https://doi.org/10.1016/j.jsg.2019.02.007>, 2019
- 17 Granado, P., Urgeles, R., Sábat, F., Albert-Villanueva, E., Roca, E., Muñoz, J.A., Mazzucca,
18 N., and Gambini, R.: Geodynamical framework and hydrocarbon plays of a salt giant:
19 the North Western Mediterranean Basin, *Petroleum Geoscience*, 22, 309-321,
20 <https://doi.org/10.1306/0323090803210.1144/petgeo2015-084>, 2016a
- 21 Granado, P., Thöny, W., Carrera, N., Gratzner, O., Strauss, P. and Muñoz, J.A.: Basement-
22 involved reactivation in fold and thrust belts: the Alpine-Carpathian Junction (Austria),
23 *Geological Magazine*, 153, 1100-1135, : <https://doi.org/10.1017/S0016756816000066>,
24 2016b
- 25 Gross, M. R.: The origin and spacing of cross joints: examples from the Monterey
26 Formation, Santa Barbara Coastline, California, *Journal of Structural Geology*, 15,
27 737-751, [https://doi.org/10.1016/0191-8141\(93\)90059-J](https://doi.org/10.1016/0191-8141(93)90059-J), 1993
- 28 Haffen, S., Géraud, Y., Diraison, M., and Dezayes, C.: Determination of fluid-flow zones in a
29 geothermal sandstone reservoir using thermal conductivity and temperature logs,
30 *Geothermics*, 46, 32-41, <https://doi.org/10.1016/j.geothermics.2012.11.001>, 2013



- 1 Iding, M., and Ringrose, P.: Evaluating the impact of fractures on the performance of the In
2 Salah CO2 storage site, *International Journal of Greenhouse Gas Control*, 4, 242-248,
3 <https://doi.org/10.1016/j.ijggc.2009.10.016>, 2010
- 4 Lash, G.G., and Engelder, T.: Jointing within the outer arc of a forebulge at the onset of the
5 Alleghanian Orogeny, *Journal of Structural Geology*, 29, 774-786,
6 <https://doi.org/10.1016/j.jsg.2006.12.002>, 2007
- 7 Laubach, S. E., Lander, R. H., Criscenti, L. J., Anovitz, L. M., Urai, J. L., Pollyea, R. M.,
8 Hooker, J. N., Narr, W., Evans, M. A., Kerisit, S. N., Olson, S. N., Dewers, T.,
9 Fisher, D., Bodnar, R., Evans, B., Dove, P., Bonnell, L. M., Marder, M. P., Pyrak-
10 Nolte, M. P.: The role of chemistry in fracture pattern development and opportunities
11 to advance interpretations of geological materials. *Reviews of Geophysics*, 57, 1065–
12 1111, <https://doi.org/10.1029/2019RG000671>, 2019
- 13 Lemiszki, P.J., Landes, J.D., and Hatcher, R.D.: Controls on hinge-parallel extension
14 fracturing in single-layer tangential-longitudinal strain folds, *Journal of Geophysical*
15 *Research: Solid Earth*, 99, 22027-22041, <https://doi.org/10.1029/94JB01853>, 1994
- 16 López-Blanco, M.: Sedimentary response to thrusting and fold growing on the SE margin of
17 the Ebro basin (Paleogene, NE Spain), *Sedimentary Geology*, 146, 133-154,
18 [https://doi.org/10.1016/S0037-0738\(01\)00170-1](https://doi.org/10.1016/S0037-0738(01)00170-1), 2002
- 19 Mardia, K.V.: Statistics of directional data. *Journal of the Royal Statistical Society. Series B*
20 (Methodological), 37, 349-393, 1975
- 21 Martinelli, M., Bistacchi, A., Balsamo, F., and Meda, M.: Late Oligocene to Pliocene
22 extension in the Maltese Islands and implications for geodynamics of the Pantelleria
23 Rift and Pelagian Platform, *Tectonics*, 38, 3394-3415,
24 <https://doi.org/10.1029/2019TC005627>, 2019
- 25 Martinez, A., Verges, J., Clavell, E., and Kennedy, J.: Stratigraphic framework of the thrust
26 geometry and structural inversion in the southeastern Pyrenees: La Garrotxa Area,
27 *Geodinamica Acta*, 3, 185-194, <https://doi.org/10.1080/09853111.1989.11105185>,
28 1989
- 29 Masciopinto, C., and Palmiotta, D.: Flow and transport in fractured aquifers: new conceptual
30 models based on field measurements, *Transport in Porous Media*, 96, 117-133, [https://](https://doi.org/10.1007/s11242-012-0077-y)
31 doi.org/10.1007/s11242-012-0077-y, 2013



- 1 Muñoz, J.A.: Evolution of a continental collision belt: ECORS-Pyrenees crustal balanced
2 cross-section. In: McClay (Ed.), Thrust Tectonics. Chapman & Hall, London, 235-246,
3 1992
- 4 Muñoz, J. A.: The Pyrenees. In: The Geology of Spain, W. Gibbons and M. T. Moreno (eds.),
5 pp. 370-385, Geological Society, London, U. K., 2002
- 6 Murray, G. H., Jr.: Quantitative fracture study - Sanish pool, McKenzie County, North
7 Dakota, AAPG Bull., 52, 57-65, 1968
- 8 Parés, J. M., van der Pluijm, B. A., and Dinarès-Turell, J.: Evolution of magnetic fabrics
9 during incipient deformation of mudrocks (Pyrenees, northern Spain), Tectonophysics,
10 307, 1-14, [https://doi.org/10.1016/S0040-1951\(99\)00115-8](https://doi.org/10.1016/S0040-1951(99)00115-8), 1999
- 11 Pujadas, J., Casas, J.M., Muñoz, J.A., and Sábat, F.: Thrust tectonics and paleogene
12 syntectonics sedimentation in the Empordà area, southeastern Pyrenees, Geodinamica
13 Acta, 3, 195-206, <https://doi.org/10.1080/09853111.1989.11105186>, 1989
- 14 Questiaux, J.-M., Couples, G.D., and Ruby, N.: Fractured reservoirs with fracture corridors,
15 Geophysical Prospecting, 58, 279-295, [https://doi.org/10.1111/j.1365-
16 2478.2009.00810.x](https://doi.org/10.1111/j.1365-2478.2009.00810.x), 2010
- 17 Quintà, A., and S. Tavani: The foreland deformation in the south-western Basque–Cantabrian
18 Belt (Spain), Tectonophysics, 576, 4-19. <https://doi.org/10.1016/j.tecto.2012.02.015>,
19 2012
- 20 Ramsay, J.G.: Folding and Fracturing of Rocks. McGraw-Hill Book Company, Inc. New
21 York. 568Pp, 1967
- 22 Ranero, C. R., Morgan, J. P., McIntosh, K., and Reichert, C.: Bending-related faulting and
23 mantle serpentinization at the Middle America trench, Nature, 425, 367-373,
24 <https://doi.org/10.1038/nature01961>, 2003
- 25 Roest, W. R., and Srivastava, S. P.: Kinematics of the plate boundaries between Eurasia,
26 Iberia, and Africa in the North Atlantic from the Late Cretaceous to the present,
27 Geology, 19, 613-616, [https://doi.org/10.1130/0091-
28 7613\(1991\)019<0613:KOTPB>2.3.CO;2](https://doi.org/10.1130/0091-7613(1991)019<0613:KOTPB>2.3.CO;2), 1991
- 29 Rosenbaum, G., Lister, G. S., and Duboz, C.: Reconstruction of the tectonic evolution of the
30 western Mediterranean since the Oligocene, Journal of the Virtual Explorer, 8, 107-
31 130, 2002



- 1 Sàbat, F., Roca, E., Muñoz, J.A., Vergés, J., Sans, M., Masana, E., Santanach, P., Estévez,
2 A., and Santisteban, C.: Role of extension and compression in the evolution of the
3 eastern margin of Iberia: the ESCI- València Trough seismic profile, *Rev. Soc. Esp.*
4 *Geol*, 8, 431-448, 1995
- 5 Santanach, P., Casas, J.M., Gratacós, O., Liesa, M., Muñoz, J.A., and Sàbat, F.: Variscan and
6 Alpine structure of the hills of Barcelona: geology in an urban area, *Journal of Iberian*
7 *Geology*, 37, 121-136, https://doi.org/10.5209/rev_JIGE.2011.v37.n2.2, 2011
- 8 Tavani, S., Storti, F., Lacombe, O., Corradetti, A., Muñoz, J. A., and Mazzoli, S.: A review of
9 deformation pattern templates in foreland basin systems and fold-and-thrust belts:
10 Implications for the state of stress in the frontal regions of thrust wedges. *Earth-*
11 *Science Reviews*, 141, 82-104, <https://doi.org/10.1016/j.earscirev.2014.11.013>, 2015
- 12 Tavani, S., Corradetti, A., De Matteis, M., Iannace, A., Mazzoli, S., Castelluccio, A.,
13 Spanos, D., and Parente, M.: Early-orogenic deformation in the Ionian zone of the
14 Hellenides: Effects of slab retreat and arching on syn-orogenic stress evolution. *Journal*
15 *of Structural Geology*, 124, 168-181, <https://doi.org/10.1016/j.jsg.2019.04.012>, 2019
- 16 Tavarnelli, E., and Peacock, D. C.: From extension to contraction in syn-orogenic foredeep
17 basins: the Contessa section, Umbria-Marche Apennines, Italy, *Terra Nova*, 11, 55-60,
18 <https://doi.org/10.1046/j.1365-3121.1999.00225.x>, 1999
- 19 Turner, J. P., and Hancock, P. L.: Relationships between thrusting and joint systems in the
20 Jaca thrust-top basin, Spanish Pyrenees. *Journal of structural geology*, 12(2), 217-226,
21 [https://doi.org/10.1016/0191-8141\(90\)90006-K](https://doi.org/10.1016/0191-8141(90)90006-K), 1990
- 22 Vegas, R.: The Valencia Trough and the origin of the western Mediterranean basins.
23 *Tectonophysics*, 203, 249-261, 1992
- 24 Vidal, J., Genter, A., and Chopin, F.: Permeable fracture zones in the hard rocks of the
25 geothermal reservoir at Rittershoffen, France, *Journal of Geophysical Research: Solid*
26 *Earth*, 122, 4864- 4887, <https://doi.org/10.1002/2017JB014331>, 2017
- 27 Whitaker, A. E., and Engelder, T.: Plate-scale stress fields driving the tectonic evolution of
28 the central Ouachita salient, Oklahoma and Arkansas, *Geological Society of America*
29 *Bulletin*, 118, 710-723, <https://doi.org/10.1130/B25780.1>, 2006



- 1 Zhao, M., and Jacobi, R.D.: Formation of regional cross-fold joints in the northern
- 2 Appalachian Plateau, *Journal of Structural Geology*, 19, 817-834,
- 3 [https://doi.org/10.1016/S0191-8141\(97\)00009-6](https://doi.org/10.1016/S0191-8141(97)00009-6), 1997
- 4

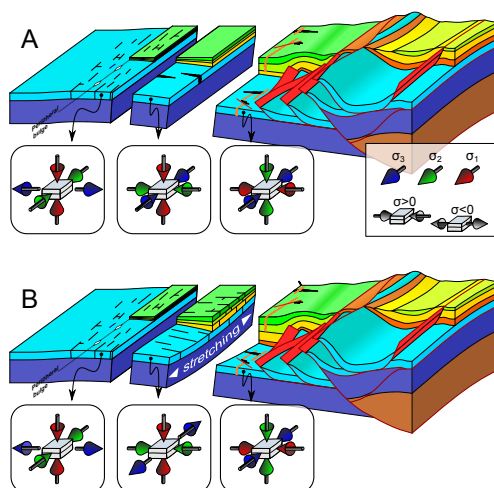


Figure 1 (Single column)

Scheme showing the architecture of a foreland fold-and-thrust belt and adjacent foredeep basin, with syn-orogenic fracture patterns in the different structural domains of the orogenic system. (A) The foredeep state of stress is governed by the permutation between the state of stress in the layer-parallel shortening and peripheral bulge domains. (B) The foredeep state of stress is controlled by the along-strike stretching of the foredeep.

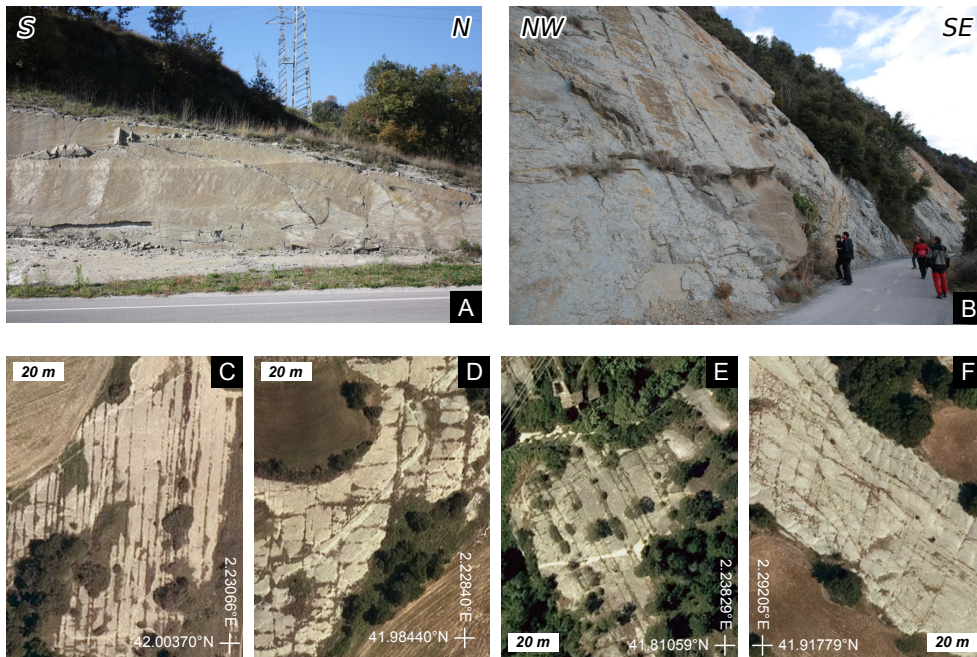


Figure 2 (Double column)

Examples of pre-folding joints within the studied area. (A) N-S striking joint with plumose structures in the foredeep sediments ($42^{\circ}02'39.7''\text{N}$; $2^{\circ}13'54.9''\text{E}$). (B) Tilted N-S striking joints in the southern limb of the Bellmunt anticline ($42^{\circ}05'39''\text{N}$; $2^{\circ}17'41.5''\text{E}$). (C to F) Examples of joints seen on orthophotos. (C) Transverse joints. (D) N-S striking transverse joints with subordinate E-W striking cross-orthogonal joints. (E) NW-SE striking joints. (F) Rare example of multiple oblique sets occurring at the same exposure. Orthophotos are available from the Spanish Instituto Geográfico Nacional (<https://pnoa.ign.es/>).

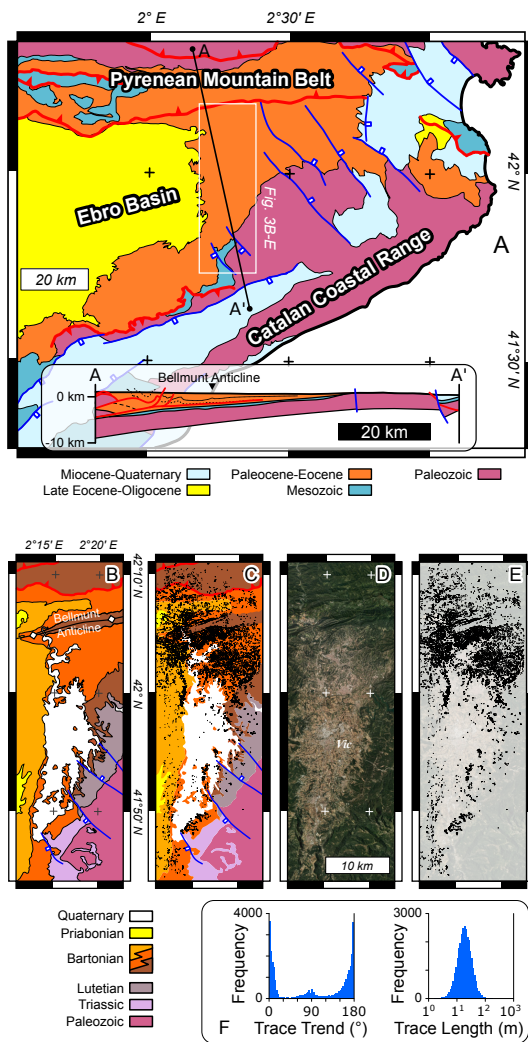


Figure 3 (Single column)

(A) Simplified geological map of the western Pyrenees and Catalan Coastal Ranges (based on the Geological Map of Catalunya scale 1:250'000; <https://www.icgc.cat/en/Downloads>), with N-S geological cross-section (modified from Parés et al., 1999). (B) Detailed geological map of the study area, with digitized joints (C). (D) Orthophoto (<https://pnoa.ign.es/>) of the study area, with digitized joints (E). (F) Frequency distribution of joint traces trend and length.

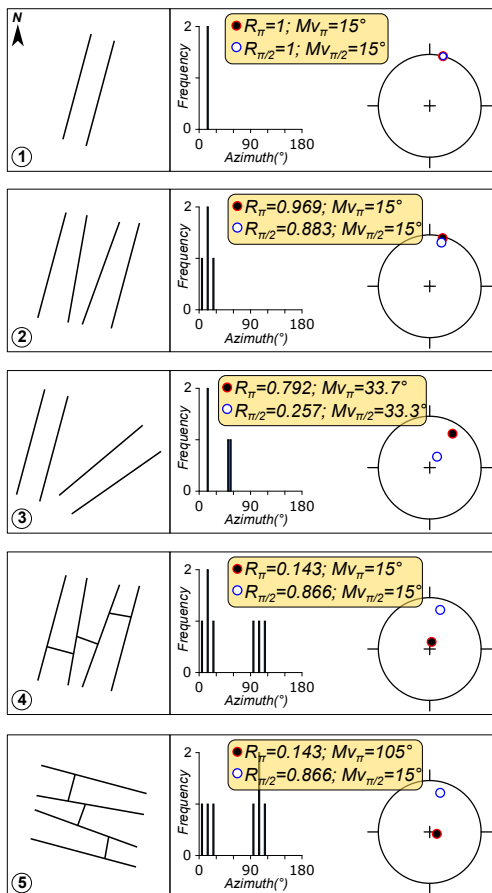


Figure 4 (Single column)

Examples of joint patterns and resultant Mv and R parameters calculated for the π and $\pi/2$ periods. For the five examples, we show the map view of the joints, the azimuthal frequency, and the sin-cos coordinates of the resultant values of Mv and R . Note that the distance from the center is proportional to R .

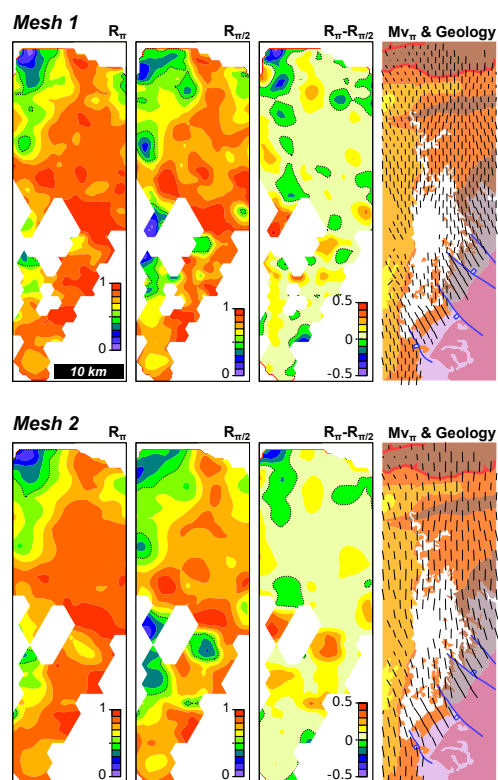


Figure 5 (Single column)
Results of circular statistics analysis for both Meshes 1 and 2. Length of traces of Mv_{π} is proportional to R_{π} . See text for details. .